Hydrol. Earth Syst. Sci. Discuss., 11, 11369–11393, 2014
www.hydrol-earth-syst-sci-discuss.net/11/11369/2014/
doi:10.5194/hessd-11-11369-2014

Hydrology and Earth System Sciences
Open Access
Discussions

Global trends in extreme precipitation: climate models vs. observations

B. Asadieh and N. Y. Krakauer

Civil Engineering Department and NOAA-CREST, The City College of the City University of New York, New York, USA

Received: 5 September 2014 – Accepted: 17 September 2014 – Published: 15 October 2014

Correspondence to: B. Asadieh (basadie00@citymail.cuny.edu)

Published by Copernicus Publications on behalf of the European Geosciences Union.

Abstract

Precipitation events are expected to become substantially more intense under global warming, but few global comparisons of observations and climate model simulations are available to constrain predictions of future changes in precipitation extremes. We present a systematic global-scale comparison of changes in historical (1901–2010) annual-maximum daily precipitation between station observations (compiled in HadEX2) and the suite of global climate models contributing to the fifth phase of the Coupled Model Inter-comparison Project (CMIP5). We use both parametric and non-parametric methods to quantify the strength of trends in extreme precipitation in observations and models, taking care to spatially and temporally sample them in comparable ways. We find that both observations and models show generally increasing trends in extreme precipitation since 1901 with largest changes in deep tropics, although annual-maximum daily precipitation has increased faster in the observations than in most of the CMIP5 models. Global average of observational annual-maximum daily precipitation has increased about 5.73 mm over the last 110 years or 8.5 % in relative terms and has increased by approximately 10 % per K of global warming since 1901, which is larger than the average of climate models with 8.3 % K^{-1}. The average rate of increase in extreme precipitation per K of warming in models and observations is higher than the rate of increase in atmospheric water vapor content per K of warming expected from the Clausius–Clapeyron equation. We expect our findings to help inform assessments of precipitation-related hazards such as flooding, droughts and storms.

1 Introduction

Trends in extreme meteorological events have received considerable attention in recent years due to the numerous extreme events such as hurricanes, droughts and floods observed (Easterling et al., 2000). Changes in global climate and alteration of Earth's hydrological cycle (Allen and Ingram, 2002; Held and Soden, 2006; Wentz et al.,

HESSD
11, 11369–11393, 2014

2007) have resulted in increased heavy precipitation with consequent increased surface runoff and flooding risk (Trenberth, 1999, 2011), which is likely to continue in the future (Dankers et al., 2013). Anthropogenic climate change is expected to change the distribution, frequency and intensity of precipitation and result in increased intensity and frequency of floods and droughts with damaging effects on environment and society (Dankers et al., 2013; Field, 2012; Min et al., 2011; O'Gorman and Schneider, 2009; Solomon et al., 2007; Trenberth, 2011; Trenberth et al., 2003).

As a result of greenhouse gas (GHG) build-up in the atmosphere, global mean near-surface temperature shows an increasing trend since the beginning of the 20th century (Angeles et al., 2007; Campbell et al., 2011; Singh, 1997; Solomon et al., 2007; Taylor et al., 2007), with greater increases in mean minimum temperature than in mean maximum temperature (Alexander et al., 2006; Peterson, 2002). The Fourth Assessment Report of Inter-Governmental Panel on Climate Change (IPCC) indicates that globally, near-surface air temperature has increased by approximately $0.74 \pm 0.18\,^{\circ}\mathrm{C}$ since 1901 with greater trend slope in recent decades (Solomon et al., 2007).

As a result of global warming, climate models and satellite observations both indicate that atmospheric water vapor content has increased at a rate of approximately $7\,\%\,\mathrm{K}^{-1}$ warming (Allen and Ingram, 2002; Held and Soden, 2006; Trenberth et al., 2005; Wentz et al., 2007), as expected from the Clausius–Clapeyron equation under stable relative humidity (Held and Soden, 2006; Pall et al., 2006). Increasing availability of moisture in the atmosphere can be expected to result in increased intensity of extreme precipitation (Allan and Soden, 2008; Allen and Ingram, 2002; O'Gorman and Schneider, 2009; Trenberth, 2011; Trenberth et al., 2003), with proportionally greater impact than for mean precipitation (Pall et al., 2006). An increase in frequency and intensity of extreme precipitation has already been identified in observations (Alexander et al., 2006; Min et al., 2011; Solomon et al., 2007; Westra et al., 2013) as well as in simulations of climate models (Kharin et al., 2013; Toreti et al., 2013). Climate models also indicate that greater increases in extreme precipitation would be expected over the next decades (Kharin et al., 2007, 2013; O'Gorman and Schneider, 2009; Pall et al.,

HESSD
11, 11369–11393, 2014

2006; Toreti et al., 2013) while moist regions become wetter and dry regions drier (Allan and Soden, 2008; Wentz et al., 2007; Zhang et al., 2007).

Although climate models generally indicate an increase in precipitation and its extremes, the rate of this increase seems to be underestimated (Allan and Soden, 2008; Allen and Ingram, 2002; Min et al., 2011; O'Gorman and Schneider, 2009; Sillmann et al., 2013; Wan et al., 2013; Wentz et al., 2007; Zhang et al., 2007), which implies that future projections of changes in precipitation extremes may also be under predicted (Allan and Soden, 2008). This underestimation can be a result of differences in scale between climate models' grids and observational data (Chen and Knutson, 2008; Sillmann et al., 2013; Toreti et al., 2013; Wan et al., 2013; Zhang et al., 2011) and/or limitations in moist convection or other parameterizations in the models (O'Gorman and Schneider, 2009; Wilcox and Donner, 2007). Assessments of climate models also reveal that the rate of increase in precipitation extremes varies greatly among models, especially in tropical zones (Kharin et al., 2007; O'Gorman and Schneider, 2009), which makes it especially important to compare modelled trends with those identified in observations. However few global comparisons of observations and climate model simulations are available to constrain predictions of future changes in precipitation extremes. Out of the available global scale studies, some use older versions of climate models or observations and/or use only one or a few climate models (Allan and Soden, 2008; Min et al., 2011; O'Gorman and Schneider, 2009; Wentz et al., 2007; Zhang et al., 2007). Temporal and spatial differences in data coverage between climate models and observations also further challenge the comparison of the results.

In this paper, we present a systematic comparison of changes in annual-maximum daily precipitation in station observations between weather stations (compiled in HadEX2) and 15 models from the suite of global climate models contributing to the latest phase of the Coupled Model Inter-comparison Project (CMIP5) (Taylor et al., 2012), as the largest and most recent set of global climate model runs. Both parametric (linear regression) and non-parametric (the Mann–Kendall as well as Sen's slope estimator) methods are utilized to quantify the strength of trends in extreme precipitation in

HESSD
11, 11369–11393, 2014

observations and models, taking care to spatially and temporally sample them in comparable ways. We also calculate the rate of change in defined extreme precipitation index per K of global warming in both observations and models to investigate the relation between global warming and precipitation extremes. Climate models and observation datasets do not provide the same temporal coverage for precipitation data, leading in some uncertainties in comparison of the results. In the present study, precipitation data for years/grids of climate models which do not have corresponding observational data are excluded, resulting in an equal weighted precipitation time series for both observations and climate models which leads into a comparable sampling approach for both datasets.

2 Data and methodology

Hadley Centre global land-based gridded climate extremes data set (HadEX2) precipitation dataset is based on daily observations from about 11 600 precipitation stations gridded on a 2.5° × 3.75° grid from 1901 to 2010 (Donat et al., 2013). Here, gridded HadEX2 annual maximum 1 day precipitation data (Rx1day) is analyzed as the observation dataset. The extreme precipitation index (Rx1day) here is defined as the annual-maximum daily precipitation, in which the maximum one day precipitation amount is selected for each year. The same index is also obtained for the climate models' simulations. Precipitation simulations of 15 models (overall 19 runs) with complete temporal data coverage have been retrieved from the fifth phase of the Coupled Model Inter-comparison Project (CMIP5) (Taylor et al., 2012), as the largest and most recent set of global climate model (GCM) runs. The historical data for projections from 1901 to 2005 and the high radiative forcing path scenario (representative concentration pathway, RCP) RCP8.5 (Moss et al., 2010) for projections from 2006 to 2010 is selected. The aforementioned 15 CMIP5 models provided by the IRI/LDEO Climate Data Library are: BCC-CSM1-1, CMCC-CM, CMCC-CMS, CNRM-CM5, GFDL-CM3, GFDL-ESM2G, HadGEM2-CC, IPSL-CM5A-LR, IPSL-CM5A-MR,

HESSD
11, 11369–11393, 2014

IPSL-CM5B-LR, MIROC5 (3 runs), MPI-ESM-LR (3 runs), MPI-ESM-MR, MRI-CGCM3 and NorESM1-M.

Climate models produce precipitation simulations for all years of a specified time interval, covering all coordinates of the globe thoroughly, even the oceans and polar zones, which is completely different from the spatial and temporal coverage of station observation datasets, such as HadEX2, where usually cover only a certain part of the continents with missing data for a considerable number of years. This results in some difficulties in comparison of the two datasets.

As a solution for this issue, a new subsampled dataset is created for each of the 19 CMIP5 climate models in which each of the HadEX2 grid-cells take the GCM precipitation data of the grid-cell that its geo-referenced coordinates fit in. The new dataset is created with the same resolution and same data availability pattern of HadEX2, which means only data of the grids/years will be assigned to the new dataset for which HadEX2 has recorded precipitation data for that year for the corresponding grid. In this way of sampling model output, if HadEX2 dataset does not have recorded precipitation data for a specified year, the newly created dataset will not have data for that year either. The newly created dataset is called the subsampled CMIP5 dataset.

As stated above, most grid-cells do not have recorded precipitation data for most of the years. A sensitivity analysis of global averaged maximum precipitation and trend slope to the minimum number of years with precipitation data required shows that these values do not change drastically (Fig. 1a and b). Selection of only stations with longer records may strengthen the confidence with which trends are quantified, but limits the calculations to smaller spatial coverage of the globe, which is not in line with scope of this study to evaluate global changes in precipitation. We chose to use only the grid-cells with at least 30 years of available precipitation data over the last 110 years, which included more than 90 % of the 766 HadEX2 data grid-cells (Fig. 1c and d).

Tests for the trend detection in climatologic time series can be classified as parametric and non-parametric methods. Parametric trend tests require independence and normal distribution in the data, while non-parametric trend tests require only that the

HESSD
11, 11369–11393, 2014

data be independent. The trend slope (b) obtained from the linear regression method is utilized for trend strength analysis and comparison of the datasets. The relative change in extreme precipitation is defined as the trend slope divided by the average of extreme precipitation of the grid-cell (b/P). The change in extreme precipitation per K of warming is also calculated as an index for the relation between changes in precipitation extremes of each grid-cell with global mean near-surface temperature, which indicates the percentage of change in extreme precipitation per K global warming. Linear regression is utilized to calculate this parameter, in which global annual mean near-surface temperature, obtained from NASA-GISS (Hansen et al., 2010) is selected as the predictor and the natural logarithm of extreme precipitation time series is chosen as response.

The Z score (Z) obtained from the Mann–Kendall test (Kendall, 1975; Mann, 1945) and Q-median (Q_{med}) from the Sen's slope estimator (Sen, 1968) are also applied in order to support the results of linear regression using non-parametric trend detection approaches. The trend tests are applied for each grid-cell's extreme precipitation time series. The obtained values have been averaged globally as well as by continent in order to present the general trend of precipitation extremes in different regions. Continents studied comprise Africa, Asia, Europe, North America, South America and Oceania. The subcontinent of India has results shown separately and is also included in Asia. Results are also averaged by latitude to investigate changes in the tropics vs. northern/southern mid-latitudes.

3 Results

Linear regression indicates that 66.2 % of the studied grids show a positive trend in annual-maximum daily precipitation during the past 110 years including 18 % that are statistically significant at 95 % confidence level. On the other hand, 33.8 % of the studied grids show a negative trend including only 4 % that are statistically significant at 95 % confidence level. Thus the global record of extreme precipitation shows a

HESSD
11, 11369–11393, 2014

meaningful increase over the last century. This increase might be expected to continue over the next decades based on physical arguments and modeling (Kharin et al., 2007, 2013; O'Gorman and Schneider, 2009; Pall et al., 2006; Toreti et al., 2013).

Table 1 presents the statistics of global averaged trend parameters of annual-maximum daily precipitation for HadEX2 and 19 subsampled CMIP5 runs (from 15 models) from 1901 to 2010. Observation is only one dataset hence it has one global average for each parameter. The 19 climate models give 19 global averages of which we present the minimum, maximum, median, mean and SD in the Table 1. Figure 2 illustrates the results presented in Table 1 as boxplots of trend parameters and average precipitation for annual-maximum daily precipitation for all 19 subsampled datasets of CMIP5 for global as well as continental scales, showing observations (HadEX2) as blue circles. The boxplots show the minimum, 25th percentile, median, 75th percentile and maximum value obtained from the climate models. As seen in Fig. 2a, the global average of extreme precipitation data shows higher value than the largest value obtained from the climate models, which indicates that all of the climate models underestimate the annual-maximum daily precipitation. This underestimation can be seen on continental scales as well and is expected given the difference in spatial scale.

The mean linear regression slope (b) for HadEX2 observation data globally shows a positive trend of 0.052 mm day^{-1} yr^{-1} in extreme precipitation over the last 110 years (Table 1). This positive trend is captured by the climate models but is significantly underestimated since HadEX2 shows a greater mean value of b than all but one of the values obtained from CMIP5 models. This underestimation is also seen in the continents of America, Europe and Oceania as well as the subcontinent of India. The global average of relative change in precipitation (b/P) for HadEX2 is close to the 75th percentile of the GCMs, which indicates that approximately 75 % of the CMIP5 models have underestimated the relative change in extreme precipitation, but is close to the average value of the models. This can be linked to the large and positive skew scatter among the results obtained from the models and the large inter-model SD (Table 1). Table 1 also shows relatively large variations of the extreme precipitation trend results

HESSD
11, 11369–11393, 2014

among the climate models in global scale. The observational relative changes in extreme precipitation for North America and Europe are higher than the maximum values obtained from the climate models, but for the South America, Oceania, Asia and Africa are lower than the median of the models suggesting that there are coherent spatial patterns in the model bias (Fig. 2).

The last column of Table 1 presents relative change in extreme precipitation per K of global warming (% K^{-1}). Global average of observed annual-maximum daily precipitation has increased by approximately 10 % per K of global warming since 1901, which is larger than the average of climate models with 8.3 % K^{-1}. The Clausius–Clapeyron equation under stable relative humidity indicates that atmospheric water vapor content will increase at a rate of approximately 7 % K^{-1} warming (Held and Soden, 2006; Pall et al., 2006). The rate of increase in extreme precipitation per K warming in both models and observations are higher than the rate of increase in atmospheric water vapor content per K warming expected from the Clausius–Clapeyron equation. Observational relative change in extreme precipitation with respect to global warming is also higher than the modelled values for the North America and Europe and is higher than the median for South America, Africa and India, but is lower than the median of the models for Asia and Oceania (Fig. 5c).

Values of Z score and Q_median indices obtained from the Mann–Kendall and Sen's trend tests, respectively, show the non-parametric confidence level of statistical significance in the identified trends in the data. The expectation might be that observational data would have lower confidence level in the identified trends due to higher level of noise in observations compared to climate model simulations. However, Table 1 shows that the global average value of Z and Q_{med} for HadEX2 is higher than the largest and second largest value obtained from the climate models, respectively, which means the CMIP5 climate models' simulations generally show lower level of confidence in the trends compared to the HadEX2 observations.

Figure 3 depicts the global maps of precipitation (P), slope (b) and relative change in precipitation (b/P) for HadEX2 (Fig. 3a–c, respectively) as well as the grid-average

HESSD
11, 11369–11393, 2014

of the subsampled CMIP5 datasets (Fig. 3d–f, respectively). Stippling means the grid-cell has a significant trend at 95 % confidence level. In cases of CMIP5 average maps, filled/empty stippling indicates positive/negative trend on average. The larger marker size means larger number of models agreeing on the presented trend, with the largest one indicating only 7 out of 19 datasets agreeing on the presented trend significance, which also illustrates the discrepancy between the climate models.

Figure 4 shows the average value of precipitation (P), trend slope (b) and relative change in precipitation (b/P) at each 2.5° latitudinal window. The figure presents the result of HadEX2 dataset with the average result of CMIP5 datasets as well as their mean ± SD. As seen in Fig. 4a, average extreme precipitation observed and simulated in the Northern Hemisphere (NH) shows a lower rate than the Southern Hemisphere (SH), and the underestimation of the extreme precipitation by the climate models can also be seen.

Tropical zones of the globe show much higher ranges of fluctuations observed and simulated for extreme precipitation trend comparing to mid-latitudes, as well as larger discrepancy between the observations and simulations (Fig. 4). There is larger uncertainty regarding the results in tropics, due to fewer numbers of cells with observational data in these regions. The failure of climate models to capture changes in tropical zones has been reported by previous studies as well (Kharin et al., 2007; O'Gorman and Schneider, 2009).

Figure 5 depicts relative change in extreme precipitation per K of global warming. The Figure depicts the maps for HadEX2 observations (Fig. 5a) and average CMIP5 (Fig. 5b), as well as box-plots of climate models (Fig. 5c) and average parameter value at each 2.5° latitudinal window (Fig. 5d).

4 Discussion

Results show that both observations and climate models show generally increasing trends in extreme precipitation intensity since 1901. Although the climate models

HESSD
11, 11369–11393, 2014

reproduce the signs observational trends on global and continental scales, the rate of change seems to be underestimated in models. Similar discrepancies between observations and climate models have also been reported in earlier studies (Allan and Soden, 2008; Allen and Ingram, 2002; Min et al., 2011; O'Gorman and Schneider, 2009; Sillmann et al., 2013; Wan et al., 2013; Wentz et al., 2007; Zhang et al., 2007). Tropical latitudes show higher ranges of fluctuations observed and simulated for extreme precipitation trends comparing to mid-latitudes, as well as larger discrepancy between the observations and simulations (Fig. 4). The high variation of the results for observations as well as models might be due to the small number of data available for those regions. However the larger discrepancy between observations and models in tropics might also be as a result of inaccuracy of the climate models in simulation of tropical climate and of precipitation generated by deep convection, as reported by previous studies (O'Gorman and Schneider, 2009). The continents of North America, Europe and Asia contain about 22, 18 and 34 % of total global data grid-cells (Fig. 1c). The trend results averaged for the continents of North America and Europe are generally in line with global averaged results. The subcontinent of India generally shows different results from the Asia average, in both observations and models (Figs. 2 and 5).

The Clausius–Clapeyron equation indicates that atmospheric water vapor content increases at a rate of $7\,\%\,K^{-1}$ of warming (Held and Soden, 2006; Pall et al., 2006). Although change in global-mean precipitation with respect to warming does not scale with the Clausius–Clapeyron equation and from energy balance consideration the rate of increase might be expected to be around $2\,\%\,K^{-1}$ (Held and Soden, 2006), impact of global warming on extreme precipitation is expected to be stronger (Pall et al., 2006). The results of the present study show that global average of extreme precipitation since 1901 has increased by approximately 10 % per K of global warming in observations and averagely $8.3\,\%\,K^{-1}$ in climate models over land areas with station observations available (Table 1). North and South America as well as Europe show even stronger increase in extreme precipitation with respect to global warming (Fig. 5). These numbers are considerably larger than the $7\,\%\,K^{-1}$ of the Clausius–Clapeyron equation which

HESSD
11, 11369–11393, 2014

further emphasizes the impact of changes in the Earth's global temperature on precipitation extremes.

As stated earlier, increased availability of moisture in the atmosphere results in greater increase in intensity of extreme precipitation than for mean precipitation (Pall et al., 2006). Faster change in extreme precipitation than mean precipitation implies the change in precipitation pattern, where the climate shifts to less rainy days and more intense precipitation. This can affect the availability of fresh water resources throughout the year. Such changes in precipitation pattern can affect the capability of reservoirs to capture excessive surface run-off and result in increased flooding events. Failure of the available reservoirs to capture the designed amounts the annual surface run-off might also result in less total annual amount of water stored in the reservoir hence less available fresh water resources. Design of the newly constructed reservoirs strongly depends on the appropriate prediction of future climate, extreme precipitations and flooding, but the available climate models seem to underestimate those.

5 Conclusions

This study presented a systematic global-scale comparison of changes in historical annual-maximum daily precipitation between the HadEX2 observational records and CMIP5 ensemble of global climate models. The climate models were spatially and temporally subsampled like the observations and trends were analyzed for grid-cells with at least 30 years of extreme precipitation data over the past 110 years. Both parametric and non-parametric methods were used to quantify the strength of trends in extreme precipitation as well as the confidence level of the identified trends. Results show that both observations and climate models show generally increasing trends in extreme precipitation since 1901 with larger changes in tropical zones, although annual-maximum daily precipitation has increased faster in the observations than in most of the CMIP5 models. Observations indicate that approximately one-fifth of the global data-covered land area had significant increasing maximum precipitation recorded during the last

HESSD
11, 11369–11393, 2014

century. This is more than 4 times larger than the areas with significant decreasing record, which indicates that the global record of extreme precipitation show a meaningful increase over the last century. Global average of observational annual-maximum daily precipitation has increased about 5.73 mm day^{-1} over the last 110 years or 8.53 % in relative terms. Global average of observational annual-maximum daily precipitation has increased by approximately 10 % per K of global warming since 1901 which is larger than the average of climate models with 8.3 % K^{-1}. The rate of increase in extreme precipitation per K of warming in both models and observations are higher than the rate of increase in atmospheric water vapor content per K of warming expected from the Clausius–Clapeyron equation which is approximately 7 % K^{-1}, which highlights the importance of extreme precipitation trends for water resources planning.

Appendix A: Non-parametric trend tests

A1 Mann–Kendall trend test

The MK test is a non-parametric rank based test (Kendall, 1975; Mann, 1945). The Mann–Kendall test statistic S is calculated as:

$$S = \sum_{i=1}^{n-1} \sum_{j=i+1}^{n} \operatorname{sgn}(x_j - x_i) \tag{A1}$$

where n is the number of data points, x_i and x_j are the data values in time series i and j ($j > i$), respectively, and sgn $(x_j - x_i)$ is the sign function:

$$\operatorname{sgn}(x_j - x_i) = \begin{cases} +1 & \text{if } x_j - x_i > 0 \\ 0 & \text{if } x_j - x_i = 0 \\ -1 & \text{if } x_j - x_i < 0 \end{cases}. \tag{A2}$$

HESSD
11, 11369–11393, 2014

The variance is computed using the equation below:

$$\mathrm{Var}\,(S) = \frac{n(n-1)(2n+5) - \sum_{i=1}^{m} t_i(t_i-1)(2t_i+5)}{18} \tag{A3}$$

where n is the number of data points, m is the number of tied groups and t_i is the number of ties of extent i. A tied group is a set of sample data having the same value. In cases where the sample size $n > 10$, the standard normal test statistic Z_S is computed as:

$$Z_S = \begin{cases} \frac{S-1}{\sqrt{\mathrm{Var}\,(S)}} & \text{if } S > 0 \\ 0, & \text{if } S = 0\,. \\ \frac{S+1}{\sqrt{\mathrm{Var}\,(S)}} & \text{if } S < 0 \end{cases} \tag{A4}$$

The sign of Z_S indicates the trend in the data series, where positive values of Z_S means increasing trend, while negative Z_S values show decreasing trends. For the tests at a specific α significance level, if $|Z_S| > Z_{1-\alpha/2}$, the null hypothesis is rejected and the time series has a statistically significant trend. $Z_{1-\alpha/2}$ is obtained from the standard normal distribution table, where at the 5 % significance level ($\alpha = 0.05$), trend is statistically significant if $|Z_S| > 1.96$ and at the 1 % significance level ($\alpha = 0.01$), trend is statistically significant if $|Z_S| > 2.576$.

A2 Sen's slope estimator

The non-parametric procedure for estimating the slope of trend in the sample of N pairs of data is developed by Sen (1968) as:

$$Q_i = \frac{x_j - x_k}{j-k} \quad \text{for } i = 1, \ldots, N \tag{A5}$$

HESSD
11, 11369–11393, 2014

where x_j and x_k are the data values at times j and k ($j > k$), respectively. N is defined as $\frac{n(n-1)}{2}$, where n is the number of time periods.

If the N values of Q_i are ranked from smallest to largest, the parameter Q_{med} is computed as the median of the Q_i vector. The Q_{med} sign reflects the direction of trend, while its value indicates the magnitude of the trend. To determine whether the median slope is statistically different than zero, the confidence interval of Q_{med} at a specific probability should be computed as follow (Gilbert, 1987; Hollander and Wolfe, 1973):

$$C_\alpha = Z_{1-\alpha/2}\sqrt{\text{Var}\,(S)} \tag{A6}$$

where Var (S) is defined before and $Z_{1-\alpha/2}$ is obtained from the standard normal distribution table. Then, $M_1 = \frac{N-C_\alpha}{2}$ and $M_2 = \frac{N+C_\alpha}{2}$ are computed. The lower and upper limits of the confidence interval, Q_{min} and Q_{max}, are the M_1 th largest and the (M_2+1)th largest of the N ordered slope estimates (Gilbert, 1987). The slope Q_{med} is statistically different than zero if the two limits Q_{min} and Q_{max} have the same sign.

The Supplement related to this article is available online at doi:10.5194/hessd-11-11369-2014-supplement.

Acknowledgements. The authors gratefully acknowledge support from NOAA under grants NA11SEC4810004 and NA12OAR4310084. All statements made are the views of the authors and not the opinions of the funding agency or the US government.

HESSD
11, 11369–11393, 2014

References

Alexander, L. V., Zhang, X., Peterson, T. C., Caesar, J., Gleason, B., Klein Tank, A. M. G., Haylock, M., Collins, D., Trewin, B., Rahimzadeh, F., Tagipour, A., Rupa Kumar, K., Revadekar, J., Griffiths, G., Vincent, L., Stephenson, D. B., Burn, J., Aguilar, E., Brunet, M., Taylor, M., New, M., Zhai, P., Rusticucci, M., and Vazquez-Aguirre, J. L.: Global observed changes in daily climate extremes of temperature and precipitation, J. Geophys. Res., 111, D05109, doi:10.1029/2005JD006290, 2006.

Allan, R. P. and Soden, B. J.: Atmospheric warming and the amplification of precipitation extremes, Science, 321, 1481–1484, doi:10.1126/science.1160787, 2008.

Allen, M. R. and Ingram, W. J.: Constraints on future changes in climate and the hydrologic cycle, Nature, 419, 224–232, doi:10.1038/nature01092, 2002.

Angeles, M. E., Gonzalez, J. E., Iii, J. E., Hern, L., National, R., and Ridge, O.: Predictions of future climate change in the caribbean region using global general circulation models, Int. J. Climatol., 27, 555–569, doi:10.1002/joc.1416, 2007.

Campbell, J. D., Taylor, M. A., Stephenson, T. S., Watson, R. A., and Whyte, F. S.: Future climate of the Caribbean from a regional climate model, Int. J. Climatol., 31, 1866–1878, doi:10.1002/joc.2200, 2011.

Chen, C.-T. and Knutson, T.: On the verification and comparison of extreme rainfall indices from climate models, J. Climate, 21, 1605–1621, doi:10.1175/2007JCLI1494.1, 2008.

Dankers, R., Arnell, N. W., Clark, D. B., Falloon, P. D., Fekete, B. M., Gosling, S. N., Heinke, J., Kim, H., Masaki, Y., Satoh, Y., Stacke, T., Wada, Y., and Wisser, D.: First look at changes in flood hazard in the Inter-Sectoral Impact Model Intercomparison Project ensemble, P. Natl. Acad. Sci. USA, 111, 3257–3261, doi:10.1073/pnas.1302078110, 2013.

Donat, M. G., Alexander, L. V., Yang, H., Durre, I., Vose, R., Dunn, R. J. H., Willett, K. M., Aguilar, E., Brunet, M., Caesar, J., Hewitson, B., Jack, C., Klein Tank, A. M. G., Kruger, A. C., Marengo, J., Peterson, T. C., Renom, M., Oria Rojas, C., Rusticucci, M., Salinger, J., Elrayah, A. S., Sekele, S. S., Srivastava, A. K., Trewin, B., Villarroel, C., Vincent, L. A., Zhai, P., Zhang, X., and Kitching, S.: Updated analyses of temperature and precipitation extreme indices since the beginning of the twentieth century: the HadEX2 dataset, J. Geophys. Res.-Atmos., 118, 2098–2118, doi:10.1002/jgrd.50150, 2013.

HESSD
11, 11369–11393, 2014

Easterling, D. R., Evans, J. L., Groisman, P. Y., Karl, T. R., Kunkel, K. E., and Ambenje, P.: Observed variability and trends in extreme climate events: a brief review, B. Am. Meteorol. Soc., 81, 417–425, doi:10.1175/1520-0477(2000)081<0417:OVATIE>2.3.CO;2, 2000.
Field, C. B.: Managing the Risks of Extreme Events and Disasters to Advance Climate Change Adaptation: Special Report of the Intergovernmental Panel on Climate Change, Cambridge University Press, Cambridge, UK, 2012.
Gilbert, R. O.: Statistical Methods for Environmental Pollution Monitoring, John Wiley & Sons, New York, USA, 1987.
Hansen, J., Ruedy, R., Sato, M., and Lo, K.: Global surface temperature change, Rev. Geophys., 48, RG4004, doi:10.1029/2010RG000345, 2010.
Held, I. M. and Soden, B. J.: Robust responses of the hydrological cycle to global warming, J. Climate, 19, 5686–5699, doi:10.1175/JCLI3990.1, 2006.
Hollander, M. and Wolfe, D. A.: Nonparametric statistical methods, J. W. & Sons, New York, USA, 1973.
Kendall, M. G.: Rank Correlation Methods, Charless Griffin, London, UK, 1975.
Kharin, V. V., Zwiers, F. W., Zhang, X., and Hegerl, G. C.: Changes in temperature and precipitation extremes in the IPCC ensemble of global coupled model simulations, J. Climate, 20, 1419–1444, doi:10.1175/JCLI4066.1, 2007.
Kharin, V. V., Zwiers, F. W., Zhang, X., and Wehner, M.: Changes in temperature and precipitation extremes in the CMIP5 ensemble, Climatic Change, 119, 345–357, doi:10.1007/s10584-013-0705-8, 2013.
Mann, H. B.: Nonparametric tests against trend, Econometrica, 13, 245–259, 1945.
Min, S.-K., Zhang, X., Zwiers, F. W., and Hegerl, G. C.: Human contribution to more-intense precipitation extremes, Nature, 470, 378–81, doi:10.1038/nature09763, 2011.
Moss, R. H., Edmonds, J. A., Hibbard, K. A., Manning, M. R., Rose, S. K., van Vuuren, D. P., Carter, T. R., Emori, S., Kainuma, M., Kram, T., Meehl, G. A., Mitchell, J. F. B., Nakicenovic, N., Riahi, K., Smith, S. J., Stouffer, R. J., Thomson, A. M., Weyant, J. P., and Wilbanks, T. J.: The next generation of scenarios for climate change research and assessment, Nature, 463, 747–756, doi:10.1038/nature08823, 2010.
O'Gorman, P. A. and Schneider, T.: The physical basis for increases in precipitation extremes in simulations of 21st-century climate change, P. Natl. Acad. Sci. USA, 106, 14773–14777, doi:10.1073/pnas.0907610106, 2009.

HESSD
11, 11369–11393, 2014

Pall, P., Allen, M. R., and Stone, D. A.: Testing the Clausius–Clapeyron constraint on changes in extreme precipitation under CO_2 warming, Clim. Dynam., 28, 351–363, doi:10.1007/s00382-006-0180-2, 2006.

Peterson, T. C.: Recent changes in climate extremes in the Caribbean region, J. Geophys. Res., 107, 4601, doi:10.1029/2002JD002251, 2002.

Sen, P. K.: Estimates of the regression coefficient based on Kendall's tau, J. Am. Stat. Assoc., 63, 1379–1389, doi:10.1080/01621459.1968.10480934, 1968.

Sillmann, J., Kharin, V. V., Zhang, X., Zwiers, F. W., and Bronaugh, D.: Climate extremes indices in the CMIP5 multimodel ensemble: Part 1. Model evaluation in the present climate, J. Geophys. Res.-Atmos., 118, 1716–1733, doi:10.1002/jgrd.50203, 2013.

Singh, B.: Climate-related global changes in the southern Caribbean: Trinidad and Tobago, Global Planet. Change, 15, 93–111, doi:10.1016/S0921-8181(97)00006-4, 1997.

Solomon, S., Qin, D., Manning, M., Marquis, M., Averyt, K., Tignor, M. M. B., Miller, H. L., and Chen, Z.: Climate Change 2007: The Physical Science Basis, Contribution of Working Group I to the Fourth Assessment Report of the Intergovernmental Panel on Climate Change, available at: http://www.ipcc.ch/pdf/assessment-report/ar4/wg1/ar4_wg1_full_report.pdf, Cambridge University Press, Cambridge, UK and New York, NY, USA, 2007.

Taylor, K. E., Stouffer, R. J., and Meehl, G. A.: An overview of CMIP5 and the experiment design, B. Am. Meteorol. Soc., 93, 485–498, doi:10.1175/BAMS-D-11-00094.1, 2012.

Taylor, M. A., Centella, A., Charlery, J., Borrajero, I., Bezanilla, A., Campbell, J., and Watson, R.: Glimpses of the future – a briefing from PRECIS Caribbean climate change project, Belmopan, Belize, 2007.

Toreti, A., Naveau, P., Zampieri, M., Schindler, A., Scoccimarro, E., Xoplaki, E., Dijkstra, H. A., Gualdi, S., and Luterbacher, J.: Projections of global changes in precipitation extremes from Coupled Model Intercomparison Project Phase 5 models, Geophys. Res. Lett., 40, 4887–4892, doi:10.1002/grl.50940, 2013.

Trenberth, K. E.: Conceptual framework for changes of extremes of the hydrological cycle with climate change, Climatic Change, 42, 327–339, doi:10.1023/a:1005488920935, 1999.

Trenberth, K. E.: Changes in precipitation with climate change, Clim. Res., 47, 123–138, doi:10.3354/cr00953, 2011.

Trenberth, K. E., Dai, A., Rasmussen, R. M., and Parsons, D. B.: The changing character of precipitation, B. Am. Meteorol. Soc., 84, 1205–1217, doi:10.1175/BAMS-84-9-1205, 2003.

HESSD
11, 11369–11393, 2014

Trenberth, K. E., Fasullo, J., and Smith, L.: Trends and variability in column-integrated atmospheric water vapor, Clim. Dynam., 24, 741–758, doi:10.1007/s00382-005-0017-4, 2005.
Wan, H., Zhang, X., Zwiers, F. W., and Shiogama, H.: Effect of data coverage on the estimation of mean and variability of precipitation at global and regional scales, J. Geophys. Res.-Atmos., 118, 534–546, doi:10.1002/jgrd.50118, 2013.
Wentz, F. J., Ricciardulli, L., Hilburn, K., and Mears, C.: How much more rain will global warming bring?, Science, 317, 233–235, doi:10.1126/science.1140746, 2007.
Westra, S., Alexander, L. V., and Zwiers, F. W.: Global increasing trends in annual maximum daily precipitation, J. Climate, 26, 3904–3918, doi:10.1175/JCLI-D-12-00502.1, 2013.
Wilcox, E. M. and Donner, L. J.: The frequency of extreme rain events in satellite rain-rate estimates and an atmospheric general circulation model, J. Climate, 20, 53–69, doi:10.1175/JCLI3987.1, 2007.
Zhang, X., Zwiers, F. W., Hegerl, G. C., Lambert, F. H., Gillett, N. P., Solomon, S., Stott, P. A., and Nozawa, T.: Detection of human influence on twentieth-century precipitation trends, Nature, 448, 461–465, doi:10.1038/nature06025, 2007.
Zhang, X., Alexander, L., Hegerl, G. C., Jones, P., Tank, A. K., Peterson, T. C., Trewin, B., and Zwiers, F. W.: Indices for monitoring changes in extremes based on daily temperature and precipitation data, WIREs Clim. Change, 2, 851–870, doi:10.1002/wcc.147, 2011.

HESSD
11, 11369–11393, 2014

Table 1. Statistics of variation of global extreme precipitation for HadEX2 and the 19 Subsampled CMIP5 models from 1901 to 2010. The table presents the statistics for the global average of the parameters. The 19 Climate models give 19 global averages of which the minimum, maximum, median, mean and SD are presented.

		Q_{med}	Z score	Slope of change (b) (mm day^{-1} yr^{-1})	Average of extreme precipitation (P) (mm day^{-1})	Relative change (b/P) (% yr^{-1})	Change per degree warming (% K^{-1})
CMIP5 (subsampled)	Model Min	0.0005	0.0944	0.0023	29.31	0.0118	4.37
	Model Max	0.0648	0.7050	0.1592	48.46	0.3849	28.67
	Model Median	0.0218	0.3056	0.0271	37.89	0.0606	7.3
	Model SD	0.0133	0.1555	0.0326	5.08	0.0774	5.16
	Model Average	0.0230	0.3330	0.0314	37.85	0.0797	8.43
HadEX2	–	0.0504	0.7242	0.0521	55.03	0.0775	9.99

HESSD
11, 11369–11393, 2014

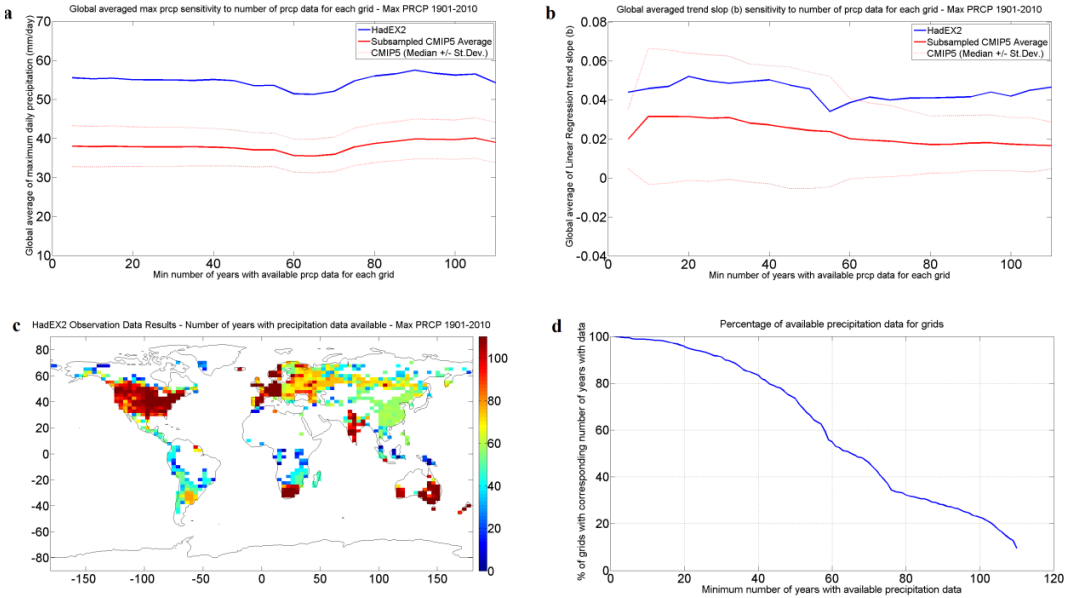

Figure 1. Minimum number of years with extreme precipitation data available vs. the global averaged extreme precipitation **(a)** and trend slope **(b)**, Map of the number of annual extreme precipitation records (1901–2010) **(c)** and minimum number of years with extreme precipitation data available vs. the percentage of the grid-cells with corresponding coverage **(d)**.

HESSD
11, 11369–11393, 2014

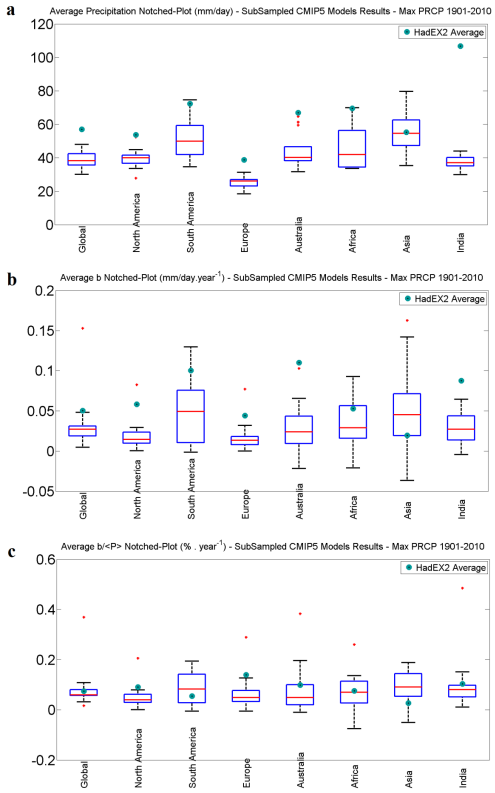

Figure 2. Boxplots of CMIP5 model run averaged results (minimum, 25th percentile, median, 75th percentile and maximum of the 19 model runs) as well as average of HadEX2 observational data (shown as blue circles) for 1901–2010 extreme precipitation data in global and continental scale – annual-averaged daily extreme precipitation (mm day^{-1}) **(a)**, slope of change in annual-averaged daily extreme precipitation (mm day^{-1} yr^{-1}) **(b)**, and relative change in annual-averaged daily extreme precipitation (% yr^{-1}) **(c)**.

HESSD
11, 11369–11393, 2014

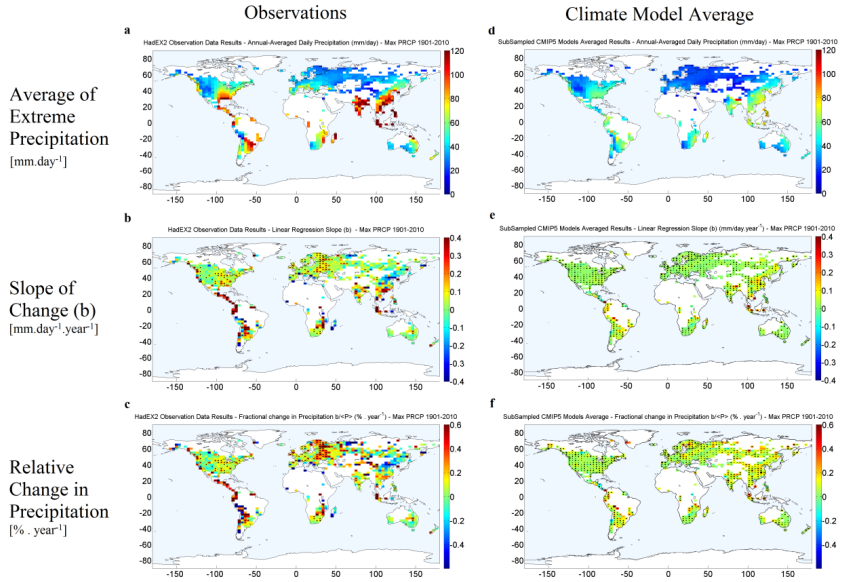

Figure 3. HadEX2 observational data vs. CMIP5 averaged results of global extreme precipitation data 1901–2010 – annual-averaged daily extreme precipitation map (mm day^{-1}) for HadEX2 **(a)** and average CMIP5 **(d)**, slope of change in annual-averaged daily extreme precipitation map (mm day^{-1} yr^{-1}) for HadEX2 **(b)** and average CMIP5 **(e)**, and relative change in annual-averaged daily extreme precipitation (% yr^{-1}) map for HadEX2 **(c)** and average CMIP5 **(f)** – the maps show the underestimation of the trends in historical extreme precipitation trends in the climate models comparing to the observations. Stippling inside the grids indicates significance of calculated trend at 95 % confidence level. In cases of CMIP5 average maps, filled/empty stippling indicates positive/negative trend on average. The larger marker size means larger number of models agreeing on the presented trend, with the largest one indicating only 7 out of 19 datasets agreeing on the presented trend significance, which also implies the discrepancy between the climate models. Maps are also shown separately in Figs. S1–6 in the Supplement.

HESSD
11, 11369–11393, 2014

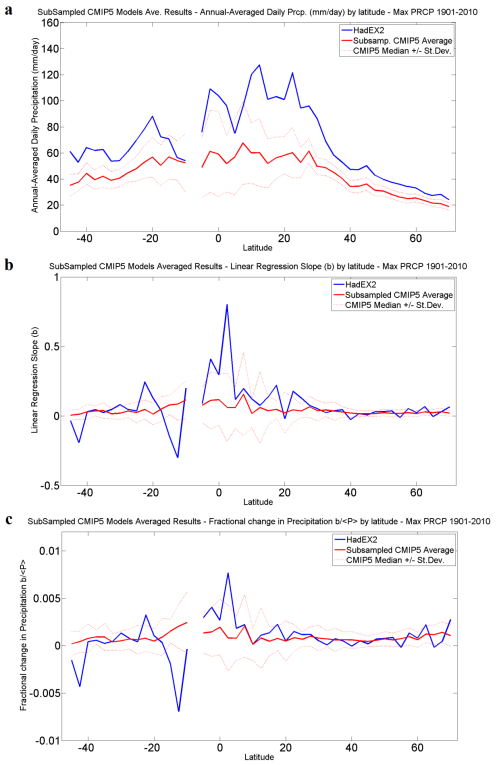

Figure 4. Average parameter value at each 2.5° latitudinal window – annual-averaged daily extreme precipitation (mm day^{-1}) for HadEX2 and average CMIP5 **(a)**, slope of change in annual-averaged daily extreme precipitation (mm day^{-1} yr^{-1}) for HadEX2 and average CMIP5 **(b)**, and relative change in extreme precipitation (% yr^{-1}) for HadEX2 and average CMIP5 **(c)**. Values for the climate models are averages of the 19 runs and the dashed lines are the median of the models plus/minus the SD of the models. The gap between the lines in the tropics indicates the lack of grid-cells with more than 30 years of precipitation data available in those zones.

HESSD
11, 11369–11393, 2014

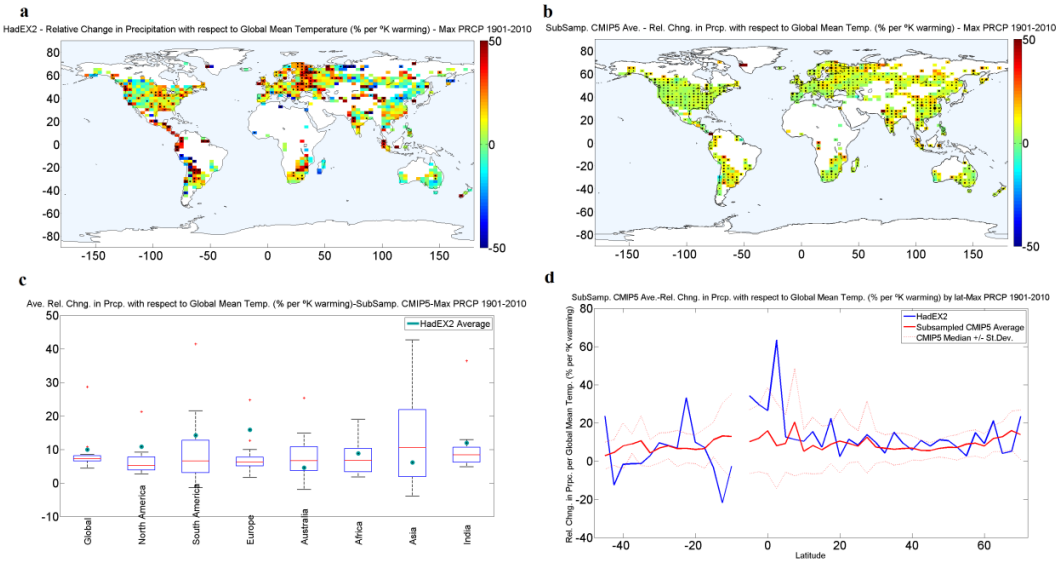

Figure 5. Relative change in extreme precipitation per K of global warming (% K^{-1}). The Figure depicts the maps for HadEX2 observations **(a)** and average CMIP5 **(b)**, as well as box-plots of climate models **(c)** and average parameter value at each 2.5° latitudinal window **(d)**. Maps are also shown separately in Figs. S7–8 in the Supplement.

HESSD
11, 11369–11393, 2014